Lattice Polarity Manipulation of Quasi-vdW Epitaxial GaN Films on Graphene through Interface Atomic Configuration

Fang Liu, Tao Wang, Zhihong Zhang, Tong Shen, Xin Rong, Bowen Sheng, Liuyun Yang, Duo Li, Jiaqi Wei, Shanshan Sheng, Xingguang Li, Zhaoying Chen, Renchun Tao, Ye Yuan, Xuelin Yang, Fujun Xu, Jingmin Zhang, Kaihui Liu*, Xin-Zheng Li*, Bo Shen, Xinqiang Wang*

Dr. F. Liu, Dr. T. Shen, Dr. X. Rong, Dr. B. W. Sheng, Dr. L. Y. Yang, D. Li, J. Q. Wei, S. S. Sheng, X. G. Li, Dr. Z. Y. Chen, Dr. R. C. Tao, Prof. X. L. Yang, Prof. F. J. Xu, Prof. K. H. Liu, Prof. X. Z. Li, Prof. B. Shen, Prof. X. Q. Wang

State Key Laboratory for Mesoscopic Physics and Frontiers Science Center for Nano-optoelectronics, School of Physics, Peking University, Beijing 100871, China.

E-mail: wangshi@pku.edu.cn; khliu@pku.edu.cn; xzli@pku.edu.cn

Prof. K. H. Liu, Prof. X. Z. Li, Prof. B. Shen, Prof. X. Q. Wang

Collaborative Innovation Center of Quantum Matter, Peking University, Beijing 100871, China

Dr. T. Wang, Prof. J. M. Zhang

Electron Microscopy Laboratory, School of Physics, Peking University, Beijing 100871, China

Prof. Z. H. Zhang

Beijing Advanced Innovation Center for Materials Genome Engineering, Beijing Key Laboratory for Magneto-Photoelectrical Composite and Interface Science, Institute for Multidisciplinary Innovation, University of Science and Technology Beijing, Beijing 100083, China.

Dr. Y. Yuan

Songshan Lake Materials Laboratory, Dongguan, Guangdong 523808, China.

Prof. K. H. Liu, Prof. X. Z. Li

Interdisciplinary Institute of Light-Element Quantum Materials, Research Center for Light-Element Advanced Materials, Peking University, Beijing 100871, China.

Prof. X. Z. Li, Prof. X. Q. Wang

Peking University Yangtze Delta Institute of Optoelectronics, Nantong, Jiangsu 226010, China.

Abstract

Quasi van der Waals (vdW) epitaxy, a pioneering epitaxy of sp^3-hybridized semiconductor films on sp^2-hybridized two-dimensional (2D) materials, provides a way, in principle, to achieve single-crystal epilayers with preferred atom configurations that are free of substrate. Unfortunately, this has not been experimentally confirmed in the case of the hexagonal semiconductor III-nitride epilayer until now. Here, for the first time, we report that the epitaxy of gallium nitride (GaN) on graphene can tune the atom arrangement (lattice polarity) through manipulation of the interface atomic configuration, where GaN films with gallium and nitrogen polarity were achieved by forming C-O-N-Ga(3) or C-O-Ga-N(3) configurations, respectively, on artificial C-O surface dangling bonds by atomic oxygen preirradiation on trilayer graphene. Furthermore, an aluminum nitride (AlN) buffer/interlayer leads to unique metal polarity due to the formation of an AlON thin layer in a growth environment containing trace amounts of oxygen, which explains the open question why those reported wurtzite III-nitride films on 2D materials always exhibit metal polarity. The reported atomic modulation through interface manipulation provides an effective model for hexagonal nitride semiconductor layer grown on graphene, which definitely promotes the development of novel semiconductor devices.

2

1. Introduction

Two-dimensional (2D) materials represented by graphene are composed of ultrathin atomic layers, and these atomic-scale monolayers (MLs) with an in-plane hexagonal honeycomb lattice are combined through van der Waals (vdW) interactions [1]. Considering their good growth compatibility with hexagonal semiconductors such as wurtzite III-nitrides [2, 3], 2D materials are regarded as an ideal platform for the fabrication of advanced (opto)electronic devices beyond the substrate limitation [4]. For instance, transferable III-nitride light-emitting diodes (LEDs) [5] and micro-LEDs [6] have been implemented on graphene, and transferable high-electron-mobility transistors (HEMTs) have been prepared on hexagonal BN [7]. Notably, these devices can be transferred from the epitaxial substrate to any other desired substrate with high heat dissipation capacity [8] or flexibility [9] and so on [10] by breaking the weak coupling interface through a simple mechanical separation method. These results demonstrate an effective method of combining commercial production equipment in the III-nitride industry, such as metal organic chemical vapor deposition (MOCVD), to intelligently manufacture flexible and/or high-power devices with low cost and high yield [11]. The breakthrough of epitaxial growth of III-nitrides on 2D materials mainly resides on the fine modulation of the weak coupling interface formed by two different hybridized systems [12], which, in principle, can achieve single-crystal epilayers with preferred atom configurations (i.e. lattice polarity) [13]. However, it has not been experimentally confirmed in the case of III-nitride epitaxy on 2D materials until now.

It is known that the sp^2-hybridized graphene surface lacks covalent dangling bonds that can serve as nucleation sites for sp^3-hybridized III-nitrides [1, 2]. Perfect vdW epitaxy actually makes the growth of relatively thick (for example, several-μm-thick) III-nitride layers, such as GaN films and device structures, very difficult since epitaxial films are easily peeled off during growth due to the weak interactions at the interface. Therefore, epitaxy of wafer-scale III-nitrides is likely quasi-vdW epitaxy, requiring defects with covalent dangling bonds; however, a lack of sufficient defects often leads to the growth of nanostructures rather than films [14]. To solve this problem, it is necessary to form some artificial dangling bonds on the surface of graphene to improve the nucleation capability of the epitaxial film [24, 25]. The quasi-vdW epitaxy of III-nitride films on 2D materials seems to have become a paradigm by first using a pretreatment method such as atomic nitrogen (N) preirradiation to form artificial dangling bonds on the surface of graphene and then adopting a high-nucleation-ability AlN buffer layer to improve the crystal quality of the film [7, 15, 16]. The epitaxial layer and graphene are actually connected in a mixed form of covalent bonds and van der Waals bonds. This paradigm, on the one hand, provides a unique opportunity to manipulate the interface and thus tune the growth

and, on the other hand, leads to an open question of why those films have unique metal lattice polarity and thus lose freedom to fabricate N-polarity based (opto-)electronic devices.

Here, we report experimental evidence for the quasi-vdW epitaxial growth of high-quality single-crystal GaN films on single-crystal graphene with controllable atom configuration. For this hexagonal semiconductor, there are two kinds of atom configurations along the c-direction due to the broken inversion symmetry, i.e., Ga- and N-lattice polarity, where each Ga atom exhibits 1 or 3 dangling bonds on the growing surface, respectively (Fig. S1). For the first time, these lattice polarities are successfully controlled by forming C-O-N-Ga(3) configuration (for Ga-polarity GaN film) or C-O-Ga-N(3) configuration (for N-polarity GaN film) on artificial C-O surface dangling bonds through atomic oxygen (O) irradiation on transferred trilayer graphene. Due to the universal applicability of this lattice polarity modulation method, it is suitable for different epitaxy methods. Furthermore, we confirmed that a few-nanometer-thick AlN buffer/interlayer leads to unique metal polarity due to the formation of an AlON ultrathin layer, which explains why the reported III-nitride films often exhibit metal polarity. This work can be seen as an effective model of atomic modulation of hexagonal nitride semiconductor films grown on layered graphene through interface manipulation, thereby promoting the industrial development of novel semiconductor devices.

2. Results and Discussion

In this work, we use plasma-assisted molecular beam epitaxy (MBE) to explore the growth behavior of wurtzite GaN films on graphene and thus to build a proper GaN/graphene interface platform. Instead of a graphene monolayer, three-monolayer-thick single-crystal graphene is used to shield the interaction between the epitaxial GaN film and the Al_2O_3 substrate. [3, 17] The schematic diagram of the epitaxial growth of GaN films on graphene is shown in Fig. 1a, which includes four steps: graphene transfer, preirradiation, GaN nucleation and GaN growth. First, three graphene monolayers were sequentially transferred to the surface of the Al_2O_3(0001) substrate. Raman scattering measurements (Fig. S2a) confirmed the fine structural quality of the transferred trilayer graphene, where the scattering peak G at 1581.9 cm^{-1} and peak 2D at 2693.1 cm^{-1} derived from graphene are obviously stronger than peak D at 1347.0 cm^{-1} arising from structural defects [18]. Then, atomic O preirradiation was applied to partially destroy the hexagonal carbon (C) lattice (Fig. S2b), thereby forming unsaturated C-O dangling bonds on the graphene surface (Fig. S2c, d). Subsequently, by providing Ga atoms and N atoms required for epitaxy, GaN nucleation started from the artificial C-O dangling bonds on the preirradiated graphene surface. Finally, GaN nucleation

islands continued to grow, coalescence, and eventually form a continuous film with an ordered hexagonal lattice arrangement. Herein, 1-μm-thick single-crystal wurtzite GaN films were grown on the transferred single crystal trilayer graphene on Al_2O_3(0001) substrates. It was found that there was an approximately 2-nm-thick gap layer composed of *in-situ* atomic O preirradiated trilayer graphene, which completely separated the epitaxial GaN film from the Al_2O_3 substrate (Fig. S3). Then, X-ray diffraction (XRD) measurements were performed to evaluate the lattice arrangement of these epitaxial GaN films. In the XRD 2θ-ω scan, the diffraction peak corresponding to the GaN (0002) plane at ~34.4° was observed (Fig. 1b). It indicates the ordered out-of-plane orientation of the GaN films. In the ϕ-scan for the (10$\bar{1}$5) plane of GaN, six peaks with an interval of 60° confirm its in-plane orientation and hexagonal symmetry (Fig. 1c). The combination of out-of-plane and in-plane orientations proves that these epitaxial GaN layers all have a regular hexagonal lattice arrangement [19]. It is worth noting that the epitaxial relation between GaN and single-crystal graphene is (0001) [10$\bar{1}$0]$_{GaN}$ || (0001) [11$\bar{2}$0]$_{graphene}$, as shown in Fig. S4a-c. Moreover, the full widths at half maximum (FWHMs) of the XRD ω-rocking curves for the (0002) and (10$\bar{1}$2) planes of the 1-μm-thick GaN film grown on the preirradiated trilayer graphene template are 0.29° and 0.35°, respectively (Fig. S4e), which are comparable to those of the film grown directly on the Al_2O_3 substrate. These results indicate that the transferred graphene layer provides the possibility of fabricating single-crystal III-nitride films with high crystal quality.

Next, we focus on this GaN/graphene epitaxial interface to explore the bonding mechanism of different hybridized materials. The interface bonding of hexagonal semiconductor GaN and graphene mainly depends on two steps shown in Fig. 1a of preirradiation and GaN nucleation, which actually determine the sequence of Ga or N atoms on the C-O surface dangling bonds on graphene, thereby forming specific interface atomic configurations as initial GaN nucleation islands. Different from the artificial C-N dangling bonds on the graphene surface, which always tend to first bind to Ga atoms to form a C-N-Ga-N(3) configuration and thus start the epitaxy of N-polarity GaN [20], the unsaturated O atoms in the C-O dangling bonds provide more GaN nucleation options. Density functional theory (DFT) calculations based on this simplified structure (Fig. 2a) were performed to clarify the interface bonding path and explore the feasible lattice polarity modulation of the epitaxial GaN film on atomic O preirradiated graphene. The essence of this simplified structure is the chemical adsorption model of Ga or N atoms on the C-O dangling bonds on the surface of monolayer graphene. More details are provided in the Tables S1, S2 and Experimental Methods. Four possible interface atomic configurations were considered: (1) one Ga atom combines with the O atom of the C-O bond (C-O-Ga), (2) one N atom combines with the O atom of the C-O bond (C-O-N), (3) one Ga

atom replaces the O atom of the C-O bond (C-Ga) and (4) one N atom replaces the O atom of the C-O bond (C-N). The calculated binding energy values of the four possible interfacial bonding paths of GaN on graphene are shown in Fig. 2b. The C-O-Ga bond is the strongest (-3.017 eV), indicating that graphene tends to initiate GaN epitaxy by binding one Ga atom on a C-O dangling bond. The C-O-N bond has the second strongest binding energy (-1.967 eV), which means that although the C-O-N bond is not as stable as the C-O-Ga bond, it can still be formed. In contrast, due to the positive binding energy values, the C-N bond (1.762 eV) and C-Ga bond (2.667 eV) are structurally unstable and cannot be formed in principle. Next, the nucleation behavior of GaN on the preferred C-O-Ga and C-O-N bonds was discussed (Fig. 2c). The Ga atom in the C-O-Ga bond has three unsaturated bonds, and it is most likely to trigger the nucleation growth of N-polarity GaN on atomic O preirradiated graphene by forming the C-O-Ga-N(3) configuration. The difference is that the N atom in the C-O-N bond tends to adsorb three Ga atoms to form the C-O-N-Ga(3) configuration and thus to initiate the epitaxy of Ga-polarity GaN on atomic O preirradiated graphene.

Following this principle, we developed a lattice polarity modulation model for epitaxial GaN films on graphene. The core technology is *in-situ* atomic O irradiation of graphene in the MBE chamber at 500 ℃ The optimization of the process parameters was briefly discussed elsewhere (Fig. S2b). By prioritizing Ga atoms rather than N atoms during high-temperature (HT) GaN growth, the nucleation and film growth of N-polarity GaN film on preirradiated graphene were realized. In detail, the shutter in front of the Ga source was opened in advance to obtain a 1-nm-thick Ga adsorption layer to protect the epitaxial interface from the destruction of N atoms provided by the N-plasma source. Then, the N-plasma source was stricken, and the epitaxy of GaN started at 780 ℃ Its polarity was confirmed by the typical (3×3) reconstructed reflection high-energy electron diffraction (RHEED) patterns (Fig. S4b) and the serious deterioration of the surface morphology (Fig. 3a) after etching with sodium hydroxide (NaOH) solution [21]. In contrast, by opening the shutter in front of the N-plasma source in advance and adopting a 5-nm-thick low-temperature (LT) GaN buffer layer at 500 ℃ the epitaxy of Ga-polarity GaN film at 780 ℃ was also achieved on preirradiated trilayer graphene/Al_2O_3 template (Fig. S4f). The Ga-polarity was confirmed by the (1×1) unconstructed RHEED patterns (Fig. S4c) and the stable surface morphology after etching with NaOH solution (Fig. 3f). It should be pointed out that the quasi-vdW epitaxy of Ga-polarity films requires a more complicated process, due to the fact that the C-O-N configuration is not stable enough (Fig. 2b). Therefore, a LT-GaN buffer layer is necessary to protect the C-O-N configuration and subsequent C-O-N-Ga(3) configuration against being broken at high temperature and thus protect the upper Ga-polarity GaN lattice arrangement. [22] Otherwise, the GaN film may eventually exhibit N-polarity due

to the dissolution of initial C-O-N/C-O-N-Ga(3) configuration and the formation of other interface bonding such as C-O-Ga-N(3) between GaN and graphene. To probe the interface bonding structure and the origin of the lattice polarity of these GaN films on the graphene template, high-resolution scanning transmission electron microscopy (STEM) measurements were performed on the N-polarity GaN film (Fig. 3c) and the Ga-polarity GaN film (Fig. 3h). For the N-polarity one, a space gap originated from 3-ML-thick graphene between the GaN film and the Al_2O_3 substrate (Fig. 3b). The integrated differential phase contrast (iDPC) STEM images of GaN near the interface region are shown in Fig. 3d, where the array of Ga and N atoms along the $[000\bar{1}]$ growth direction indicates the N lattice polarity. Moreover, as shown in Fig. 3e, this N-polarity lattice arrangement is likely to start from the GaN/graphene interface with a discontinuous monolayer of O atoms (i.e., the C-O dangling bonds on trilayer graphene surface). [23] This is consistent with the calculation results of N-polarity GaN on graphene through the expected C-O-Ga-N(3) configuration (Fig. 2c). The following STEM measurements of the Ga-polarity film on trilayer graphene further confirm the interfacial atomic model based on the calculation results (Fig. 3g, i). Notably, the Ga lattice polarity of the film results from the GaN/graphene interface, where GaN is most likely to bond with the uppermost graphene through a discontinuous O atomic layer (Fig. 3j), i.e., the expected C-O-N-Ga(3) configuration. Therefore, theoretical prediction (Fig. 2) coincides with the experimental results (Fig. 3, Fig. S4), which indicates that the hexagonal lattice of the epitaxial GaN film is determined by the three-monolayer-thick single-crystal graphene layer rather than the substrate and that the lattice polarity is modulated by the interfacial atomic configuration between GaN and graphene. Thus far, we have achieved the quasi-vdW epitaxy of wurtzite GaN films and established a lattice polarity modulation model of epitaxial GaN films on graphene through interfacial atomic configuration.

Notably, this model does not depend on the epitaxy technique. Herein, we also realized the epitaxy of both Ga- and N-polarity GaN films on atomic O-preirradiated trilayer single-crystal graphene through MOCVD (Fig. S5). In this case, we used ammonia (NH_3) as the N source and a relatively thick LT-GaN buffer layer to protect the expected interface atomic configuration and prevent it from being destroyed at higher growth temperatures. In addition, we can achieve the separation of quasi-vdW epitaxial GaN film from the Al_2O_3 substrate with the help of thermal release tape (Fig. S4f, g). Because of this lattice polarity modulation model of epitaxial GaN on graphene through interfacial atomic configuration rather than the lattice arrangement of the substrate, we were able to achieve the desired GaN-based epitaxial structures for multifunctional devices on various substrates.

Considering that our MBE system is used for the epitaxy of nitride and oxide semiconductors, the oxygen content in the chamber may be slightly higher than that of the conventional MBE system.

From this viewpoint, the growth ambient is somehow close to that of MOCVD. Finally, we would like to answer the open question of why the GaN layer grown by MOCVD on graphene and some other 2D materials with the help of an AlN buffer layer always exhibits Ga lattice polarity. To eliminate the disturbance of the imperfect graphene surface and slightly disordered AlN nucleation conditions, we designed an experiment using a GaN/AlN/GaN sandwich structure grown on an atomic O-preirradiated trilayer graphene/Al_2O_3 template by plasma-assisted MBE (Fig. 4a). Here, before AlN epitaxy, an approximately 100-nm-thick GaN layer was grown on the transferred trilayer graphene/Al_2O_3 template by the expected C-O-Ga-N(3) configuration to obtain an atomic-scale clear AlN/GaN interface. According to the lattice polarity modulation model of epitaxial GaN discussed above, this structure should have N lattice polarity, similar to the results shown in Fig. 3d. However, this method does not seem to be suitable for this GaN/AlN/GaN sandwich structure because the bottom GaN has N-polarity (Fig. 4d), while the upper GaN has Ga polarity (Fig. 4b, c). In other words, the AlN interlayer reverses the lattice polarity of GaN from N lattice polarity to Ga lattice polarity. Further iDPC-STEM measurements (Fig. 4e) show that the lattice polarity of the AlN interlayer is indeed reversed from N- to Al-polarity near the spatial position approximately 3 nm above the AlN/GaN interface. To illustrate this unusual lattice polarity reversal mechanism, high-angle annular dark-field (HAADF) STEM and energy-dispersive X-ray spectroscopy (EDX) measurements were performed on this AlN/GaN interface. As shown in Fig. 4f, there is obvious enrichment of the O composition near the lattice polarity inversion region in AlN compared with GaN or upper AlN, as confirmed by the contrast difference. An EDX line scan performed along the marked direction shows that the average atomic O fraction increased from ~0.03 (AlN in the white area and GaN in the gray area) to ~0.08 (AlN in the gray area), as depicted in Fig. 4g. However, the atomic N fraction and atomic O fraction exhibited opposite trends with the spatial position. Even at three specific points of AlN in the gray area, the atomic O fraction obviously increased to ~0.20, and the atomic N fraction decreased to ~0.14 (marked by the black arrow). The enriched O atoms will tend to partially replace the N atoms in the hexagonal AlN lattice to form a thin AlON layer. The 5-monolayer-thick O-rich AlN layer with an obvious contrast difference with the surroundings (Fig. 4h) further proved this viewpoint, where the upper AlN has Al-polarity, and the bottom AlN has N-polarity. Considering the structure of this AlON thin layer [22, 24], we can propose a reasonable lattice polarity reversal model in the AlN interlayer (Fig. 4i). Since the precise ratio of O and N components is difficult to directly determine, we used two-color balls to represent nonmetallic atoms. For N-polarity AlN, the higher surface chemical activity facilitates the incorporation of higher fractions of O atoms [25], which in turn forms a few-nm-thick AlON layer and thus reverses the lattice polarity of the

8

upper AlN to a relatively chemically inert metal polarity. The metal polarity in the AlN layer is mainly related to the incorporation of O atoms from the epitaxial environment, epitaxial substrates and source materials, which is somehow free of growth equipment. It has been reported that the MOCVD-grown AlN layer on pretreated graphene initially has nitrogen lattice polarity through the C-N dangling bond to form C-N-Al-N(3) configuration, and then reverses to the metal lattice polarity by forming a thin AlON layer. [15, 19] In other words, in MOCVD growth, a small amount of oxygen leads to formation of AlON layer which locks metal lattice polarity of the upper epilayer. Therefore, the lattice polarity modulation of epitaxial GaN on graphene reported in this manuscript provides freedom for fabricating multifunctional devices based on III-nitrides with both kinds of lattice polarities.

3. Conclusion

In summary, we have demonstrated the lattice polarity manipulation of quasi-vdW epitaxial GaN on graphene by interfacial atomic configuration engineering. By using atomic O preirradiation and atomic Ga and N supply sequences to form the C-O-N-Ga(3) and C-O-Ga-N(3) configurations, N- and Ga-lattice polarity GaN films were achieved on transferred graphene, respectively. This polarity-control rule is not affected by growth methods such as MBE and MOCVD and is free of either crystalline or noncrystalline substrates. It makes epitaxy of wurtzite III-nitrides with preferred lattice polarity possible on graphene according to objective demands and definitely improves the capability to fabricate more kinds of devices with multiple functions, which are believed to play an important role in next-generation semiconductor devices.

4. Experimental Methods

Graphene synthesis and transfer: Monolayer single-crystal graphene was grown on a single-crystal Cu(111) substrate by chemical vapor deposition (CVD). The growth of graphene was conducted at 1030 ℃ The detailed procedure is described in the previous report. [26] Then, trilayer graphene templates were achieved by the polymethyl methacrylate (PMMA)-mediated transfer method. Monolayer graphene/Cu was first spin-coated with PMMA (950 K, 4.0 wt% in ethyl lactate). The PMMA/graphene film was pasted onto another graphene/Cu sample after etching the Cu substrate (etchant: 4.0 wt% $(NH_4)_2S_2O_8$ aqueous solution). By repeating the above process again and then removing the Cu substrate, free-standing PMMA/trilayer graphene was obtained. Finally, the dried PMMA/trilayer graphene was transferred onto the Al_2O_3(0001) substrate, and the PMMA was removed by hot acetone (70 ℃.

Graphene preirradiation: The transferred graphene templates were kept at 500 ℃ in a plasma-assisted MBE chamber with an O-plasma source. Then, 3 min of atomic O preirradiation was performed with an O_2 flow rate of 0.8 standard cubic centimeters per minute (sccm) and a radio frequency plasma power of 250 W to form unsaturated C-O dangling bonds on the trilayer graphene surface as nucleation sites for wurtzite GaN epitaxy (Fig. S2b). The C-O dangling bonds formed on the surface of preirradiated graphene can be first combined with Ga or N atoms, which makes possible the fine modulation of the interfacial atomic configuration between the GaN film and the graphene.

Theoretical Simulation: DFT calculations were implemented by the Vienna ab initio Simulation Package (VASP) code. Projector augmented wave (PAW) pseudopotentials were used for electron–ion interactions. The generalized gradient approximation (GGA) was used for the exchange correlation functional as proposed by Perdew–Burke–Ernzerhof (PBE). The energy cutoff for plane wave expansion was 600 eV. In the calculation, a 4×4×1 Γ centered k-point mesh was used, and spin polarization was considered. This monolayer graphene unit cell model contained a 20 Å vacuum layer along the c-axis direction to avoid any interactions between periodic images. The lattice parameters of the graphene unit cell were a = b = 2.468 Å, $\alpha = \beta = 90°$, and $\gamma = 120°$. More detailed information is provided in Support Information (S6).

MBE growth of wurtzite GaN films: (1) N-polarity GaN films grown on atomic O preirradiated trilayer graphene. In the MBE growth chamber, approximately 3 ML Ga atoms were first supplied by a thermal evaporation source before HT-GaN epitaxy at 780 ℃. Then, the N-plasma source was stricken, and bottom GaN films were deposited at 780 ℃ The deposition process is described as follows: turn on the shutters of Ga source for 6 s, the corresponding beam equivalent pressure was approximately $5.5×10^{-7}$ mbar; then turn on the shutter of N-plasma source for 30 s to provide sufficient N atoms to combine with Ga atoms to form bottom GaN (the N_2 flow rate was 0.25 sccm, and the plasma power was 220 W); repeat the above steps 10 times (about 10-monolayer-thick GaN) to protect the expected C-O-Ga-N(3) configuration. Finally, 1-μm-thick N-polarity GaN films were deposited at 780 ℃ with a growth rate of approximately 3 nm/min. During GaN epitaxy, the N_2 flow rate was 0.8 sccm, the plasma power was 350 W, and the beam equivalent pressure of the Ga atomic beam was approximately $5.5×10^{-7}$ mbar. (2) Ga-polarity GaN films grown on atomic O preirradiated trilayer graphene. According to theoretical guidance, 5 s of gentle atomic nitrogen treatment was first performed at 500 ℃ to form an expected C-O-N configuration. Then, a LT-GaN buffer/protection layer (5-nm-thick) was finely deposited at 500 ℃ in which the shutter in front of the Ga source was opened 3 s earlier than that of the N-plasma sources. During the abovementioned steps, the N_2 flow rate was 0.25 sccm, the radio frequency plasma power was 220 W, and the beam

10

equivalent pressure of the Ga atomic beam was approximately 5.0×10^{-8} mbar. The small N atomic beam is mainly used to protect these fragile interface states on the graphene surface. Considering the influence of growth temperature on the thermal evaporation rate of Ga atoms on the graphene surface, the Ga beam current here for LT-GaN epitaxy is also smaller. Subsequently, 1-μm-thick Ga-polarity GaN films were deposited at 780 ℃. During GaN deposition, the N_2 flow rate was 0.8 sccm, the plasma power was 350 W, and the beam equivalent pressure of the Ga atomic beam was approximately 5.5×10^{-7} mbar. (3) Epitaxy of AlN interlayer. The AlN interlayer was deposited at 780 ℃ and its growth rate was approximately 3 nm/min. During AlN deposition, the N_2 flow rate was 0.8 sccm, the plasma power was 350 W, and the beam equivalent pressure of the Al atomic beam was approximately 2.5×10^{-7} mbar.

Characterization: The structural quality of transferred graphene was characterized by Raman scattering spectroscopy using a 532 nm laser (CNI MSL-200 mW) as the excitation source and a HORIBA-iHR550 spectrometer. XPS (Kratos, Axis Supra) was performed to quantitatively estimate the chemical composition of graphene before and after atomic oxygen activation. The surface morphology of epitaxial GaN film on the graphene template and the morphology of the GaN film after etching by NaOH solution (10%, AR) at 60°C for 20 min were measured by AFM in tapping mode (Bruker Dimension ICON-PT). High-resolution spherical aberration-corrected STEM characterization was performed using an FEI Titan Cubed Themis G2 300.

Supporting Information

Supporting Information is available from the Wiley Online Library or from the author.

Acknowledgements

References

[1] A. K. Geim, K. S. Novoselov, *Nat Mater* **2007**, *6*, 183; X. Z. Xu, Z. H. Zhang, L. Qiu, J. N. Zhuang, L. Zhang, H. Wang, C. N. Liao, H. D. Song, R. X. Qiao, P. Gao, Z. H. Hu, L. Liao, Z. M. Liao, D. P. Yu, E. G. Wang, F. Ding, H. L. Peng, K. H. Liu, *Nat Nanotechnol* **2016**, *11*, 930; Y. Kubota, K. Watanabe, O. Tsuda, T. Taniguchi, *Science* **2007**, *317*, 932; H. Yu, M. Z. Liao, W. J. Zhao, G. D. Liu, X. J. Zhou, Z. Wei, X. Z. Xu, K. H. Liu, Z. H. Hu, K. Deng, S. Y. Zhou, J. A. Shi, L. Gu, C. Shen, T. T. Zhang, L. J. Du, L. Xie, J. Q. Zhu, W. Chen, R. Yang, D. X. Shi, G. Y. Zhang, *ACS Nano* **2017**, *11*, 12001; A. Koma, *Thin Solid Films* **1992**, *216*, 72.

[2] K. Chung, C. H. Lee, G. C. Yi, *Science* **2010**, *330*, 655; J. W. Ben, X. K. Liu, C. Wang, Y. P. Zhang, Z. M. Shi, Y. P. Jia, S. L. Zhang, H. Zhang, W. J. Yu, D. B. Li, X. J. Sun, *Adv Mater* **2021**, *33*, 2006761; J. H. Park, X. Yang, J. Y. Lee, M. D. Park, S. Y. Bae, M. Pristovsek, H. Amano, D. S. Lee, *Chem Sci* **2021**, *12*, 7713.

[3] W. Kong, H. S. Li, K. Qiao, Y. Kim, K. Lee, Y. F. Nie, D. Lee, T. Osadchy, R. J. Molnar, D. K. Gaskill, R. L. Myers-Ward, K. M. Daniels, Y. W. Zhang, S. Sundram, Y. Yu, S. H. Bae, S. Rajan, Y. Shao-Horn, K. Cho, A. Ougazzaden, J. C. Grossman, J. Kim, *Nat Mater* **2018**, *17*, 999.

[4] J. Kim, C. Bayram, H. Park, C. W. Cheng, C. Dimitrakopoulos, J. A. Ott, K. B. Reuter, S. W. Bedell, D. K. Sadana, *Nat Commun* **2014**, *5*, 4836; Y. Kim, S. S. Cruz, K. Lee, B. O. Alawode, C. Choi, Y. Song, J. M. Johnson, C. Heidelberger, W. Kong, S. Choi, K. Qiao, I. Almansouri, E. A. Fitzgerald, J. Kong, A. M. Kolpak, J. Hwang, J. Kim, *Nature* **2017**, *544*, 340; P. K. Mohseni, A. Behnam, J. D. Wood, X. Zhao, K. J. Yu, N. C. Wang, A. Rockett, J. A. Rogers, J. W. Lyding, E. Pop, X. L. Li, *Adv Mater* **2014**, *26*, 3755; H. Oh, Y. J. Hong, K. S. Kim, S. Yoon, H. Baek, S. H. Kang, Y. K. Kwon, M. Kim, G. C. Yi, *NPG Asia Mater* **2014**, *6*, e145.

[5] N. Han, T. V. Cuong, M. Han, B. D. Ryu, S. Chandramohan, J. B. Park, J. H. Kang, Y. J. Park, K. B. Ko, H. Y. Kim, H. K. Kim, J. H. Ryu, Y. S. Katharria, C. J. Choi, C. H. Hong, *Nat Commun* **2013**, *4*, 1452.

[6] J. Jeong, Q. X. Wang, J. Cha, D. K. Jin, D. H. Shin, S. Kwon, B. K. Kang, J. H. Jang, W. S. Yang, Y. S. Choi, J. Yoo, J. K. Kim, C. H. Lee, S. Lee, A. A. Zakhidov, S. Hong, M. J. Kim, Y. J. Hong, *Sci Adv* **2020**, *6*, eaaz5180.

[7] N. R. Glavin, K. D. Chabak, E. R. Heller, E. A. Moore, T. A. Prusnick, B. Maruyama, D. E. Walker, D. L. Dorsey, Q. Paduano, M. Snure, *Adv Mater* **2017**, *29*, 1701838; M. J. Motala, E. W. Blanton, A. Hilton, E. Heller, C. Muratore, K. Burzynski, J. L. Brown, K. Chabak, M. Durstock, M. Snure, N. R. Glavin, *ACS Appl Mater Inter* **2020**, *12*, 21837.

[8] T. Ayari, S. Sundaram, X. Li, Y. El Gmili, P. L. Voss, J. P. Salvestrini, A. Ougazzaden, *Appl Phys Lett* **2016**, *108*, 171106.

[9] G. Yang, Y. Jung, C. V. Cuervo, F. Ren, S. J. Pearton, J. Kim, *Opt Express* **2014**, *22*, A812.

[10] Y. Kobayashi, K. Kumakura, T. Akasaka, T. Makimoto, *Nature* **2012**, *484*, 223; H. Kum, D. Lee, W. Kong, H. Kim, Y. Park, Y. Kim, Y. Baek, S. H. Bae, K. Lee, J. Kim, *Nat Electron* **2019**, *2*, 439.

[11] Y. Yu, T. Wang, X. F. Chen, L. D. Zhang, Y. Wang, Y. F. Niu, J. Q. Yu, H. T. Ma, X. M. Li, F. Liu, G. Q. Deng, Z. F. Shi, B. L. Zhang, X. Q. Wang, Y. T. Zhang, *Light-Sci Appl* **2021**, *10*, 117; Y. Qi, Y. Y. Wang, Z. Q. Pang, Z. P. Dou, T. B. Wei, P. Gao, S. S. Zhang, X. Z. Xu, Z. H. Chang, B. Deng, S. L. Chen, Z. L. Chen, H. N. Ci, R. Y. Wang, F. Z. Zhao, J. C. Yan, X. Y. Yi, K. H. Liu, H. L. Peng, Z. Q. Liu, L. M. Tong, J. Zhang, Y. J. Wei, J. M. Li, Z. F. Liu, *J Am Chem Soc* **2018**, *140*, 11935; X. Li, S. Sundaram, Y. El Gmili, T. Ayari, R. Puybaret, G. Patriarche, P. L. Voss, J. P. Salvestrini, A. Ougazzaden, *Cryst Growth Des* **2016**, *16*, 3409.

[12] D. D. Liang, T. B. Wei, J. X. Wang, J. M. Li, *Nano Energy* **2020**, *69*, 104463; J. D. Yu, L. Wang, Z. B. Hao, Y. Luo, C. Z. Sun, J. Wang, Y. J. Han, B. Xiong, H. T. Li, *Adv Mater* **2020**, *32*, 1903047.

[13] M. Hetzl, M. Kraut, T. Hoffmann, M. Stutzmann, *Nano Lett* **2017**, *17*, 3582; P. Wang, Y. Yuan, C. Zhao, X. Q. Wang, X. T. Zheng, X. Rong, T. Wang, B. W. Sheng, Q. X. Wang, Y. Q. Zhang, L. F. Bian, X. L. Yang, F. J. Xu, Z. X. Qin, X. Z. Li, X. X. Zhang, B. Shen, *Nano Lett* **2016**, *16*, 1328.

[14] H. Yoo, K. Chung, Y. S. Choi, C. S. Kang, K. H. Oh, M. Kim, G. C. Yi, *Adv Mater* **2012**, *24*, 515; I. M. Hoiaas, A. Liudi Mulyo, P. E. Vullum, D. C. Kim, L. Ahtapodov, B. O. Fimland, K. Kishino, H.

13

Weman, *Nano Lett* **2019**, *19*, 1649; V. Kumaresan, L. Largeau, A. Madouri, F. Glas, H. Z. Zhang, F. Oehler, A. Cavanna, A. Babichev, L. Travers, N. Gogneau, M. Tchernycheva, J. C. Harmand, *Nano Lett* **2016**, *16*, 4895; S. Fernandez-Garrido, M. Ramsteiner, G. H. Gao, L. A. Galves, B. Sharma, P. Corfdir, G. Calabrese, Z. D. Schiaber, C. Pfuller, A. Trampert, J. M. J. Lopes, O. Brandt, L. Geelhaar, *Nano Lett* **2017**, *17*, 5213; J. Jeong, D. K. Jin, J. Cha, B. K. Kang, Q. X. Wang, J. Choi, S. W. Lee, V. Y. Mikhailovskii, V. Neplokh, N. Amador-Mendez, M. Tchernycheva, W. S. Yang, J. Yoo, M. J. Kim, S. Hong, Y. J. Hong, *ACS Appl Nano Mater* **2020**, *3*, 8920; A. KovACS, M. Duchamp, R. E. Dunin-Borkowski, R. Yakimova, P. L. Neumann, H. Behmenburg, B. Foltynski, C. Giesen, M. Heuken, B. Pecz, *Adv Mater Interfaces* **2015**, *2*, 1400230.

[15] Z. L. Chen, Z. Q. Liu, T. B. Wei, S. Y. Yang, Z. P. Dou, Y. Y. Wang, H. N. Ci, H. L. Chang, Y. Qi, J. C. Yan, J. X. Wang, Y. F. Zhang, P. Gao, J. M. Li, Z. F. Liu, *Adv Mater* **2019**, *31*, 1807345.

[16] J. Ning, C. C. Yan, Y. Q. Jia, B. Y. Wang, Y. Zeng, J. C. Zhang, D. Wang, Y. Hao, *ACS Appl Nano Mater* **2020**, *3*, 5061; Y. Chen, H. Zang, K. Jiang, J. W. Ben, S. L. Zhang, Z. M. Shi, Y. P. Jia, W. Lu, X. J. Sun, D. B. Li, *Appl Phys Lett* **2020**, *117*, 051601; P. Wang, A. Pandey, J. Gim, W. J. Shin, E. T. Reid, D. A. Laleyan, Y. Sun, D. H. Zhang, Z. Liu, Z. H. Zhong, R. Hovden, Z. T. Mi, *Appl Phys Lett* **2020**, *116*, 171905.

[17] S. Zhang, B. Y. Liu, F. Ren, Y. Yin, Y. Y. Wang, Z. L. Chen, B. Jiang, B. Z. Liu, Z. T. Liu, J. Y. Sun, M. Liang, J. C. Yan, T. B. Wei, X. Y. Yi, J. X. Wang, J. M. Li, P. Gao, Z. F. Liu, Z. Q. Liu, *Small* **2021**, *17*, 210098; F. Ren, B. Y. Liu, Z. L. Chen, Y. Yin, J. Y. Sun, S. Zhang, B. Jiang, B. Z. Liu, Z. T. Liu, J. W. Wang, M. Liang, G. D. Yuan, J. C. Yan, T. B. Wei, X. Y. Yi, J. X. Wang, Y. Zhang, J. M. Li, P. Gao, Z. F. Liu, Z. Q. Liu, *Sci Adv* **2021**, *7*, eabf5011.

[18] J. H. Lee, E. K. Lee, W. J. Joo, Y. Jang, B. S. Kim, J. Y. Lim, S. H. Choi, S. J. Ahn, J. R. Ahn, M. H. Park, C. W. Yang, B. L. Choi, S. W. Hwang, D. Whang, *Science* **2014**, *344*, 286.

[19] Y. X. Feng, X. L. Yang, Z. H. Zhang, D. Kong, J. Zhang, K. H. Liu, X. Z. Li, J. F. Shen, F. Liu, T. Wang, P. F. Ji, F. J. Xu, N. Tang, T. J. Yu, X. Q. Wang, D. P. Yu, W. K. Ge, B. Shen, *Adv Funct Mater* **2019**, *29*, 1905056.

[20 F. Liu, Z. H. Zhang, X. Rong, Y. Yu, T. Wang, B. W. Sheng, J. Q. Wei, S. Y. Zhou, X. L. Yang, F. J. Xu, Z. X. Qin, Y. T. Zhang, K. H. Liu, B. Shen, X. Q. Wang, *Adv Funct Mater* **2020**, *30*, 2001283.

[21] G. Naresh-Kumar, J. Bruckbauer, A. Winkelmann, X. Yu, B. Hourahine, P. R. Edwards, T. Wang, C. Trager-Cowan, R. W. Martin, *Nano Lett* **2019**, *19*, 3863.

[22] S. Mohn, N. Stolyarchuk, T. Markurt, R. Kirste, M. P. Hoffmann, R. Collazo, A. Courville, R. Di Felice, Z. Sitar, P. Vennegues, M. Albrecht, *Phys Rev Appl* **2016**, *5*, 054004.

[23] Z. P. Dou, Z. L. Chen, N. Li, S. Y. Yang, Z. W. Yu, Y. W. Sun, Y. H. Li, B. Y. Liu, Q. Luo, T. B. Ma, L. Liao, Z. F. Liu, P. Gao, *Nat Commun* **2019**, *10*, 5013.

[24] H. Yang, J. G. Lozano, T. J. Pennycook, L. Jones, P. B. Hirsch, P. D. Nellist, *Nat Commun* **2015**, *6*, 7266.

[25] N. Stolyarchuk, T. Markurt, A. Courville, K. March, J. Zuniga-Perez, P. Vennegues, M. Albrecht, *Sci Rep* **2018**, *8*, 14111; D. Wang, K. Uesugi, S. Y. Xiao, K. Norimatsu, H. Miyake, *Appl Phys Express* **2020**, *13*, 095501.

[26] X. Z. Xu, Z. H. Zhang, J. C. Dong, D. Yi, J. J. Niu, M. H. Wu, L. Lin, R. K. Yin, M. Q. Li, J. Y. Zhou, S. X. Wang, J. L. Sun, X. J. Duan, P. Gao, Y. Jiang, X. S. Wu, H. L. Peng, R. S. Ruoff, Z. F. Liu, D. P. Yu, E. G. Wang, F. Ding, K. H. Liu, *Sci Bull* **2017**, *62*, 1074.
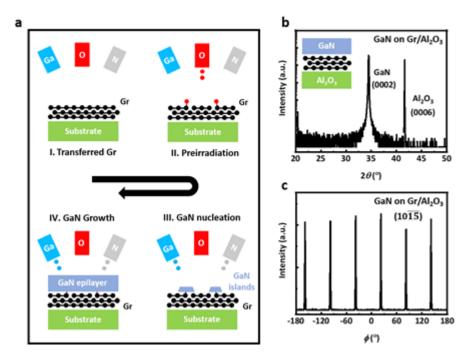
Figure 1. Epitaxial growth of a hexagonal semiconductor GaN film on layered graphene. (**a**) Schematic diagram of the growth process of wurtzite GaN films on graphene (Gr), including (I) transfer of Gr, (II) preirradiation, (III) GaN nucleation and (IV) GaN growth. (**b**) XRD 2θ-ω scan of a 1-µm-thick GaN film grown on a trilayer graphene/Al_2O_3(0001) substrate by MBE. (**c**) XRD azimuthal off-axis ϕ-scan for the GaN ($10\overline{1}\overline{5}$) reflection confirming its six-fold symmetry.
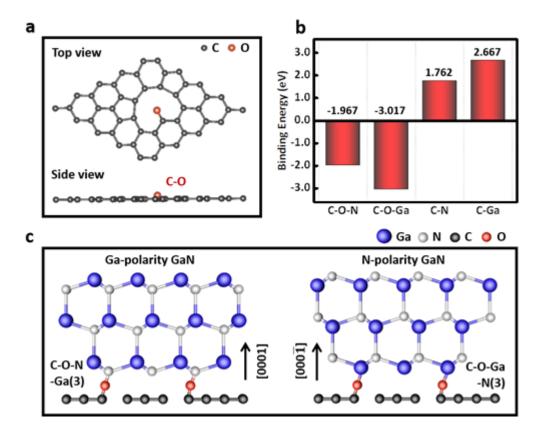
Figure 2. Theoretical calculation of the hexagonal semiconductor GaN/graphene interface bonding configuration. (**a**) Top-view and side-view diagrams of the optimized structure of a single O atom chemisorbed on a graphene monolayer. **(b)** Calculated binding energy values of various cases of one Ga or N atom absorption on a monolayer graphene surface through an unsaturated C-O bond. (**c**) Schematic diagram of the lattice polarity modulation mechanism of wurtzite GaN films grown on graphene through the preferred interface configuration, where the C-O-N configuration tends to adsorb three Ga adoms to from C-O-N-Ga(3) configuration, and the C-O-Ga configuration tends to adsorb three N atoms to from C-O-Ga-N(3) configuration. Herein, the C-O-N-Ga(3) configuration always corresponds to Ga-polarity GaN, and the C-O-Ga-N(3) configuration always corresponds to N-polarity GaN.
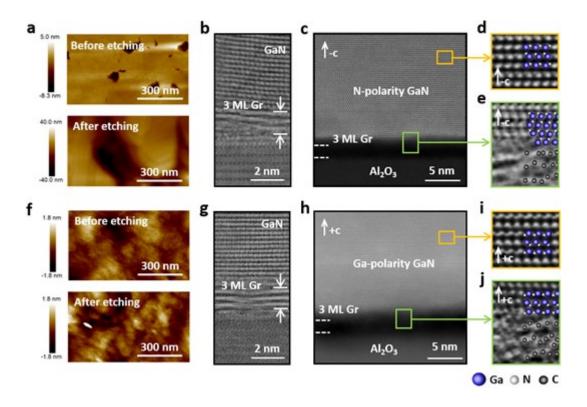
Figure 3. Exploration of the interface atomic structure of epitaxial GaN films on graphene. (**a**) AFM images of a 1-µm-thick epitaxial GaN film grown on a trilayer graphene/Al_2O_3(0001) template via the expected C-O-Ga-N(3) configuration before and after NaOH solution etching. The surface deterioration phenomenon during etching is due to the high surface chemical activity of the N-polarity film. (**b**, **c**) iDPC-STEM and HAADF-STEM images of the interface atomic structure of this N-polarity film. The adhesion between the graphene and the Al_2O_3 substrate is not perfect, causing the graphene surface to fluctuate, which leads to the tilt of the GaN lattice in some areas. (**d**, **e**) iDPC-STEM images of the lattice arrangement of this N-polarity GaN film. (**f**) AFM images of a 1-µm-thick Ga-polarity GaN film on a trilayer graphene/Al_2O_3 template through the expected C-O-N-Ga(3) configuration before and after NaOH solution etching. (**g**, **h**) iDPC-STEM and HAADF-STEM images of the interface atomic structure of this Ga-polarity film. The slightly blurred interface may come from structural damage caused by the high-energy electron beam during STEM measurement. (**i**, **j**) iDPC images of the lattice arrangement of this Ga-polarity film. Herein, these images (**b-e**, **g-j**) viewing both along the [11$\bar{2}$0] orientation of GaN. The [000$\bar{1}$] growth direction of N-polarity GaN is marked as the -c direction, and the [0001] growth direction of Ga-polarity GaN is marked as the +c direction.
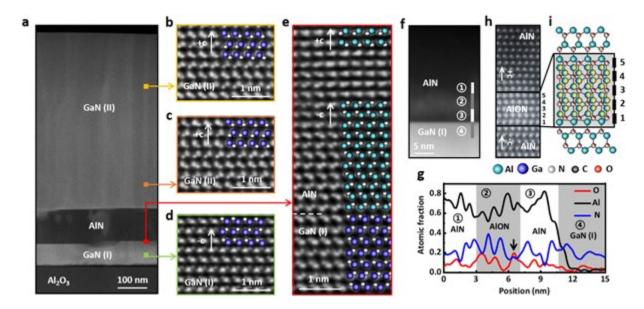
Figure 4. Lattice polarity reversal effect of the AlN interlayer on the upper III-nitride layer. (**a**) HAADF-STEM image of the epitaxial GaN/AlN/GaN sandwich structure on an atomic O preirradiated trilayer graphene/Al_2O_3(0001) template through the expected C-O-Ga-N(3) configuration. (**b-d**) iDPC-STEM images of the bottom GaN (I) and upper GaN (II) layers, where the bottom layer has N-polarity and the upper layer has Ga-polarity. (**e**) An iDPC-STEM image of the AlN/GaN interface area, showing the lattice polarity inversion phenomenon existing in the AlN insertion layer. (**f**) A HAADF-STEM image and (**g**) an EDX line scan analysis performed on the AlN/GaN interface showing the enrichment of O atoms in the polarity inversion region of the AlN interlayer. (**h**) A HAADF-STEM image and (**i**) a schematic diagram of the AlN layer above the GaN interface, including the planar inversion domain boundary. Since it is impossible to accurately confirm the ratio of O and N atoms at each position, the N lattice positions in the ideal AlN are filled with two-color small balls to represent AlON. The yellow parts of these Al atom balls indicate possible vacancies. Herein, these images (**a-f, h**) viewing both along the [11$\bar{2}$0] orientation of GaN.

Herein, we report the manipulation of the lattice polarity of quasi-vdW epitaxial GaN on graphene through controlling interface bonding form. This polarity-control rule is not affected by growth methods and is free of either crystalline or non-crystalline substrates. It makes the epitaxy of III-nitrides with preferred lattice polarity possible and definitely improves the ability to fabricate advanced semiconductor devices.

Fang Liu, Tao Wang, Zhihong Zhang, Tong Shen, Xin Rong, Bowen Sheng, Liuyun Yang, Duo Li, Jiaqi Wei, Shanshan Sheng, Xingguang Li, Zhaoying Chen, Renchun Tao, Ye Yuan, Xuelin Yang, Fujun Xu, Jingmin Zhang, Kaihui Liu*, Xin-Zheng Li*, Bo Shen, Xinqiang Wang*

Lattice Polarity Manipulation of Quasi-vdW Epitaxial GaN Films on Graphene through Interface Atomic Configuration